Molecular Spectroscopy

Valentina Watanabe
21367661
Lab partner: Ellen Lyons

January 2025

I have read and understood the plagiarism provisions in the General Regulations of the University Calendar for the current year, found at http://www.tcd.ie/calendar. I have also read and understood the guide, and completed the 'Ready Steady Write' Tutorial on avoiding plagiarism, located at https://libguides.tcd.ie/academic-integrity/ready-steady-write.

Signed: 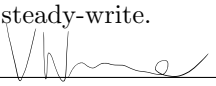 Date: 05/02/2025

Contents

1 Abstract

Molecular spectroscopy is a crucial analytical tool for understanding the structural and dynamic properties of molecules. We analyze the emission spectrum of nitrogen (N_2), iodine (I_2) and continuum white light. Key molecular transitions were identified, providing insights into electronic and vibrational energy levels. The nitrogen emission spectrum exhibited vibrational energy spacing reduction, confirming molecular anharmonicity, while vibrational transitions were identified using the spectra peaks, which proved to follow the Franck-Condon principle. The iodine absorption spectrum revealed electronic excitation transitions, though heating inconsistencies affected spectral clarity. Additionally, the tungsten-halogen lamp spectrum was compared to blackbody radiation, highlighting instrumental sensitivity variations.

2 Introduction

Molecular spectroscopy is a key tool for studying the energy structure of molecules by analyzing their interaction with light. This method provides crucial insights into the electronic, vibrational, and rotational transitions that define molecular behavior. The total energy of a molecule consists of three main components: electronic, vibrational, and rotational energies, each of which corresponds to specific spectral transitions. These transitions occur when molecules absorb or emit photons, causing changes in their energy states.

This experiment explores the absorption and emission spectra of nitrogen (N_2), iodine (I_2) and continuum white light to investigate electronic and vibrational transitions. Using Flame-T and Flame-S spectrometers, the experiment captures spectral data, identifying key molecular parameters such as vibrational frequencies and their relation to Franck-Condon factors. The results provide insight into molecular energy levels, anharmonicity, and the overlap of vibrational wavefunctions.

3 Theory

3.1 Molecular Spectroscopy

Spectroscopy measures the different levels of energy. In molecular spectroscopy, the focus of the study is molecular vibrations and their interactions with electromagnetic radiation at different wavelengths (Bersohn & Berne, 2003). Transitions between different energy levels happen because of the absorption or emission of photons. The sum of the total energy of a molecule is formed by electronic E_n, vibrational E_v, and rotational E_j energies, eq.(1).

$$E = E_n + E_v + E_j \tag{1}$$

Using spectroscopy we can further observe each unique molecular spectra, in elements such as Nitrogen and Iodine, to draw important conclusions about the transitions of the three mentioned types of energies. After identifying the observed peaks associated with specific absorption or emission transitions and determining their corresponding wavenumbers, it becomes possible to compute the fundamental vibration frequency of this anharmonic oscillator, along with the anharmonicity constant and bond force constant, and to visualize the potential energy curve of the bond (Trinity College Dublin, 2023).

Electronic transitions occur when an electron moves between molecular orbitals, usually within the ultraviolet (UV) and visible regions of the spectrum. The energy associated with an electronic transition is given by:

$$\Delta E = h\nu \tag{2}$$

where h is Planck's constant and ν is the frequency of the absorbed or emitted radiation (Herzberg, 1950).

3.2 Vibrational Energy

In low energy levels, can model the vibrations of molecules as a mass on a spring. By Hooke's Law, the restorative force follows $F = -kx$, with energy potential,

$$V(x) = \frac{1}{2}kx^2 \tag{3}$$

By solving Schdrodinger's equation we find the energy to be,

$$E_\nu = \left(\nu + \frac{1}{2}\right)\hbar\omega \tag{4}$$

Here, ν is the principal quantum number, ω is the fundamental frequency of the oscillation defined as $\omega = \sqrt{\frac{k}{\mu}}$ with μ as the reduced mass and k as the spring constant. To analyze molecular vibrations, it is useful to express the fundamental frequency in terms of the wavenumber $\tilde{\nu}$. Since frequency ν and angular frequency ω are related by,

$$\nu = \frac{\omega}{2\pi} \tag{5}$$

we substitute this into the equation for wavenumber, knowing that:

$$\tilde{\nu} = \frac{\nu}{c} \tag{6}$$

Thus, we obtain:

$$\tilde{\nu} = \frac{\omega}{2\pi c} \tag{7}$$

The wavenumber of the fundamental frequency of the vibration $\tilde{\nu}$ is the reciprocal of the wavelength, so it has units of inverse centimetres (cm^{-1}). We can also convert this to energy by using Planck's equation $E = h\nu$. Since frequency is related to wavenumber by

$$\nu = c\tilde{\nu} \tag{8}$$

we replace and obtain:

$$E = hc\tilde{\nu} \tag{9}$$

For most scenarios, like in high energy levels, this approximation is not functioning. Instead, we use the Morse Potential, an anharmonic oscillator with an asymmetric potential:

$$V(r) = D_e\left(1 - e^{-\beta(r-r_0)}\right)^2 \tag{10}$$

D_e is the depth of the potential well, r is the internuclear distance, r_0 is the equilibrium distance between the two nuclei and β is proportional to $\tilde{\nu}$ by,

$$\tilde{\nu} = \frac{1}{2\pi c}\sqrt{\frac{k}{\mu}} = \frac{\beta}{c}\sqrt{\frac{D_e}{2\pi^2\mu}} \tag{11}$$

(Trinity College Dublin, 2023).

Vibrational transitions occur because of changes in the bond length, modelled by the harmonic and anharmonic oscillator approximations.

3.3 Rotational Energy

Besides the vibrational motion of molecules, these also present rotational movements. Rotational transitions are associated with the rotation of the molecule about its centre of mass. These follow the rigid rotor model, a model that explains rotating systems. In classical mechanics, the energy of rotation can be expressed as

$$E = \frac{P^2}{2I} \tag{12}$$

where P is angular momentum P = $I\omega$ and I is moment of inertia $\sum_i m_i r_i^2$ (Herzberg, 1950).

To determine the possible energy levels according to quantum theory we solve Schrodinger's Equation to find the energy to be,

$$E_J = \frac{J(J+1)\hbar^2}{2I} \tag{13}$$

J being the rotational quantum numbers J = 0,1,2, $\cdots$. F(J) is then the rotational term in cm^{-1} given by,

$$F(J) = \frac{E_J}{hc} = -\frac{h}{8\pi^2 cI}J(J+1) = BJ(J+1), \tag{14}$$

with constant B

$$B = \frac{h}{8\pi^2 cI} \tag{15}$$

(Herzberg, 1950).

Due to the spectrometers' limited resolution, detecting the rotational component in the spectra is not possible in this experiment. Instead, the observed spectra will consist of a combination of electronic and vibrational transitions, known as vibronic transitions.

3.4 Molecular Bonding

When atoms join to form molecules, their distinct atomic orbitals merge to produce molecular orbitals. This can occur via constructive or destructive interference of their wave functions, resulting in the formation of bonding and anti-bonding orbitals, respectively. The characteristics of these orbitals play an important role in defining the stability, electronic configuration, and spectroscopic attributes of the molecule.

The key differences between bonding and anti-bonding orbitals can be understood by analyzing the charge density distribution ρ which represents the probability of finding an electron in a given region as seen in Figure 1. As it can be observed, bonding orbitals Ψ_+ are formed by the constructive interference of atomic

orbitals. There is higher electron density between the nuclei which causes an increase in electron probability in the bonding region, which strengthens the bond. This also results in a more stable molecule as it has lower energy states. On the other hand, anti-bonding orbitals Ψ_- are formed by destructive interference, which causes zero electron density between nuclei. The lower electron density destabilizes the molecule. It causes higher energy states so a less stable molecule.

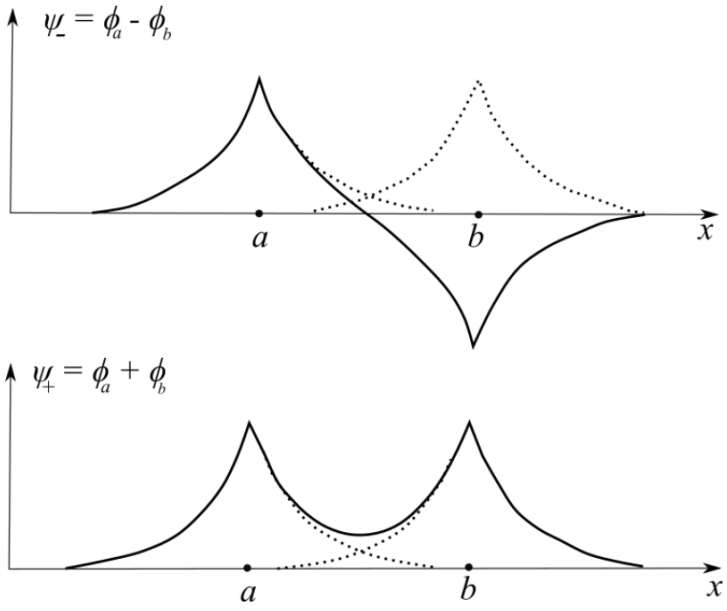

Figure 1: Wavefunctions for an anti-bonding orbital (top) and bonding orbital (bottom) in the simplest case of a hydrogen molecule showing atomic 1s orbitals in each case. (Trinity College Dublin, 2023).

This experiment examines how molecules transition between energy states by analyzing both emission and absorption spectra. For Nitrogen, we attempt to observe electronic de-excitations, where molecules release energy as they move from higher-energy excited states to lower-energy molecular states, producing an emission spectrum. This process directly relates to molecular orbitals, as electrons transition from higher-energy anti-bonding orbitals to lower-energy bonding orbitals, resulting in spectral lines. To determine the corresponding energy transitions to the vibrational levels we use Diagram 2,

Conversely, for Idoine, we observe electronic excitations, where molecules absorb specific wavelengths of light to promote electrons from lower-energy bonding orbitals to higher-energy anti-bonding orbitals, generating an absorption spectrum. This absorption corresponds to transitions from the molecular ground state to excited electronic states, revealing information about the energy structure of the molecule.

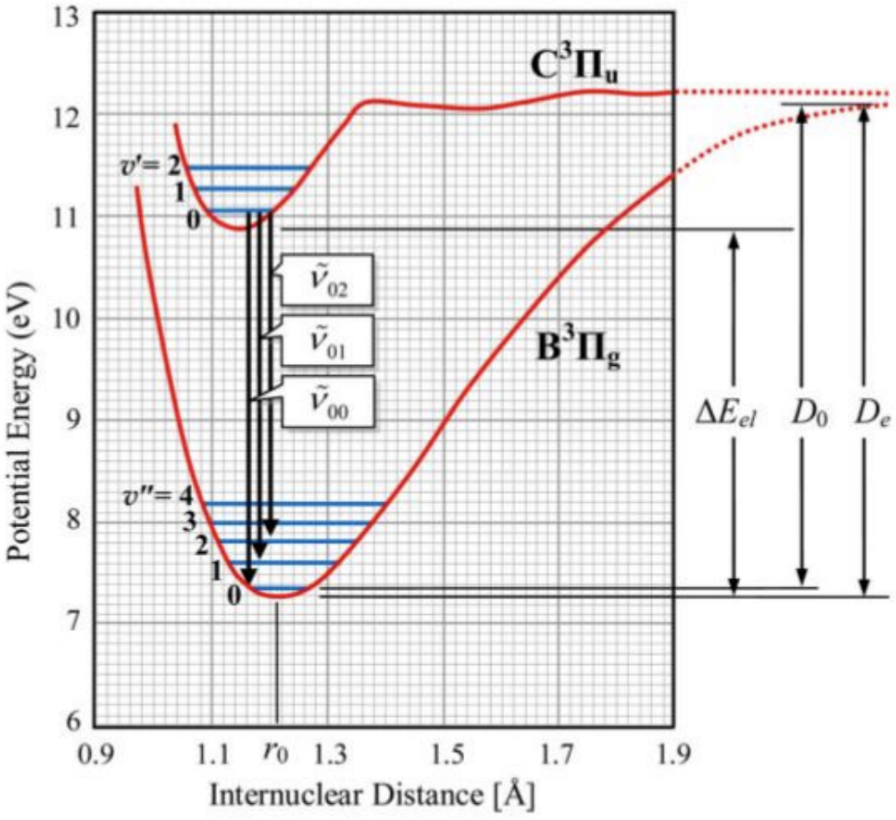

Figure 2: Potential energy diagram of Nitrogen $C^3\Pi_u$ and $B^3\Pi_u$ molecular levels with vibrational levels ν' and ν'' respectively.

3.5 Vibronic Transitions and Franck-Condon Factors

Vibrational and electronic transitions often occur simultaneously in what are known as vibronic transitions. The intensity of these transitions depends on the overlap of vibrational wavefunctions between two electronic states, described by the Franck-Condon principle, given by the factor:

$$P_{mn} \propto \left| \int \psi_m^*(r)\psi_n(r)\, dr \right|^2 \tag{16}$$

Ψ_m and Ψ_n are the vibrational wavefunctions of the initial and final states and r is the nuclear coordinate or distance (Trinity College Dublin, 2023). The integral measures the extent of overlap between vibrational states. This principle explains why some transitions are more intense than others.

Table 1 gives several Franck-Condon factors which help us identify the peaks of the N_2 spectrum. A larger FCF means a higher transition probability and greater intensity in the spectrum. The strongest spectral lines correspond to transitions where there is maximum overlap between the vibrational wave functions of the initial and final states. This often corresponds to 0 - 0 transitions.

$\nu' \setminus \nu''$	0	1	2	3	4	5	6	7
0	4527	3291	1462	517.2	158.8	45.4	12.2	3.2
1	3949	215.7	2033	1989	1097	466.3	171	56.8
2	1330	3413	238.4	634.4	1605	1393	791	362
3	202	2530	2110	890	50	936	1310	987
4	9	537	3300	1160	1160	34.8	402	1010

Table 1: Table of Franck-Condon factors for N_2. (Trinity College Dublin, 2023).

Vibronic transitions, as mentioned previously, refer to simultaneous changes in both electronic and vibrational energy states within a molecule. Unlike purely electronic transitions, which involve the movement of an electron between molecular orbitals, vibronic transitions also account for the interaction between the electronic states and molecular vibrations (Atkins & Friedman, 2005). The energy of a vibronic transition is given by:

$$\tilde{\nu}_{\nu',\nu''} = \tilde{\nu}_{00} + \tilde{\nu}_C\nu' - \tilde{\nu}_B\nu'' - \tilde{\nu}_C x_C(\nu'+1)\nu' + \tilde{\nu}_B x_B(\nu''+1)\nu'' \tag{17}$$

where

$$\tilde{\nu}_{00} = \tilde{\nu}_{el} + \frac{1}{2}(\tilde{\nu}_C - \tilde{\nu}_B) - \frac{1}{4}(x_B\tilde{\nu}_B - x_C\tilde{\nu}_C) \tag{18}$$

and ν_{el} is the electronic transition energy, ν_c, x_c, ν_b, x_b, are vibrational parameters for the upper (C) and lower (B) states.

4 Experimental Method

4.1 Setup

In this experiment, we analyze the emission and absorption spectra of nitrogen (N_2) and iodine (I_2) utilizing two different spectrometers. The first one is a Flame-T Spectrometer, used for recording emission spectra in the range 300–510 nm. The second one is the Flame-S Spectrometer, used for recording absorption spectra in the range 350–850 nm. Both spectrometers are crossed Czerny-Turner type, which means that they are configured for a particular arrangement of optics in a spectrograph, which is designed for rapid spectral acquisition (JPierce, 2017). They are connected to a computer and controlled using OceanView software. The light is input through a 50 μm diameter optical fiber which removes the need for an input slit. The spectrometer records spectra via a Charge-Coupled Device (CCD) array, which converts detected photons into an electronic signal through an Analog-to-Digital Converter (ADC).

4.2 Experiment 1

The aim of this first experiment is to gather the emission spectrum of a mercury discharge lamp to record and analyze it, using the Flame-T and Flame-S Spectrometer. Through this, we are also able to calibrate the spectrometers by comparing the measured spectral lines of mercury with known reference values. Additionally, we can draw key spectrometer properties, including wavelength calibration, resolving power, and

spectral resolution.

The calibration procedure was first performed with a spectral range of 300 - 510 nm. As stated, both spectrometers were connected to the computer via USB. The optical fiber was securely mounted on a retort stand, positioned to collect light from the mercury discharge lamp. We take into consideration four factors: integration time, averaging, boxcar smoothing, and dark current correction. The four main controls are adjusted while observing the results to enhance the reading and optimize the spectral data.

Once the spectrometer settings were optimized, using first the Flame-T and then the Flame-S, the emission spectrum of mercury was recorded. Spectral lines can be identified using the cursor tool in the OceanView software. The wavelengths of spectral peaks are recorded and then a comparison with standard values is drawn.

The spectrometer resolution and resolving power are obtained. The optical resolution of any peak is the full width at half maximum (FWHM) of the peak. The chromatic resolving power, R, is defined as

$$R = \frac{\lambda}{\Delta\lambda} \tag{19}$$

where $\Delta\lambda$ is the minimum wavelength difference that can be distinguished by the spectrometer. It was measured as the FWHM of selected spectral peaks. A visualization of this is portrayed in Figure 3.

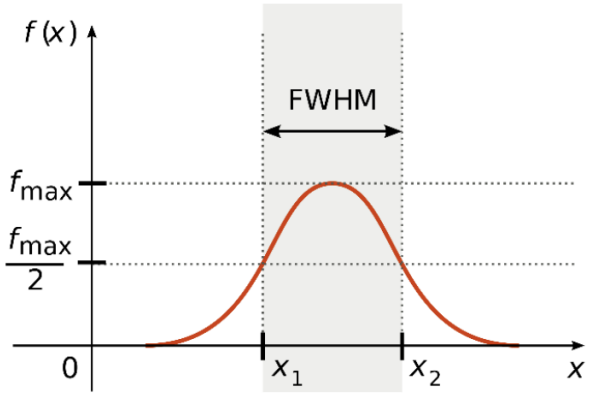

Figure 3: Visualization of the FWHM (Trinity College, 2023)

4.3 Experiment 2

The second part of this laboratory experiment aimed to record and analyze the molecular emission spectrum of Nitrogen (N_2). The spectral outcome of excited gas, using a nitrogen discharge lamp, allows us to investigate the vibrational transitions within its electronic states. To do so, the Flame-T spectrometer was used to capture the spectrum which permitted for an analysis of the Franck-Condon principle and vibrational structure in the observed bands. Since the nitrogen lamp produces intense emission, careful attention was given to integration time settings to prevent saturation. The lamp was operated for a maximum of 15 minutes per session to prevent overheating, as indicated by the laboratory safety guidelines.

The integration time was carefully set to ensure that spectral peaks were well-defined without exceeding

the detector's limits. If the integration time was too low, the peaks would be weak and difficult to distinguish. Meanwhile, excessive integration time led to saturation, which clipped the intensity of the emission lines. As in the previous section, scan averaging was applied to reduce random noise. The number of scans per average was again set to five, ensuring a smooth spectrum while maintaining reasonable data acquisition time.

Once the optimal parameters were determined, the molecular nitrogen spectrum was recorded. The strongest transition, corresponding to the 0-0 vibrational band, and the Franck-Condon factors tables were used as a reference for identifying additional vibronic transitions. This was further used to create a Deslandres table. The data was then saved for further analysis.

4.4 Experiment 3

In experiment 3 the aim is to evaluate the wavelength sensitivity of a spectrometer by studying the emission spectrum of a continuum white light source, namely a tungsten halogen lamp, using the Flame-S spectrometer. As in experiment 1, we first record the differing effects of changing the variables of integration time, averaging parameter, boxcar setting, and selecting "correct for electrical dark".

To obtain the sensitivity as a function of wavelength, we first obtain the Intensity spectrum after adjusting the required parameters. Because the mission of this tungsten halogen lamp is that of a black body radiator with a temperature of 2800 K, we can use the wavelength values provided and find the plot for a simulated black body emission spectrum. To do so, we use the formula

$$I(\lambda) = \frac{2\pi hc^2}{\lambda^5 \left(\exp\left(\frac{hc}{\lambda kT}\right) - 1\right)} \tag{20}$$

To finally compute the 'sensitivity' S, we plot the measured intensity over the blackbody intensity.

4.5 Experiment 4

The final part of the laboratory comprised of finding the absorption spectrum of molecular iodine. The experiment was conducted using a tungsten-halogen lamp as the broad-spectrum light source. This light was directed through a heating iodine vapor cell where the iodine molecules absorbed specific wavelengths corresponding to allowed electronic and vibrational transitions. The transmitted light was then collected and analyzed using a Flame-S spectrometer, which operates in the 350–850 nm range. Additionally, a collimating lens was placed at the output of the light source to ensure uniform beam propagation through the iodine cell. The light that passed through the iodine vapor was then focused onto the spectrometer's fiber optic cable, ensuring efficient light collection. Heating the cell causes the Iodine to sublimate and produce I_2 vapour, which with an increase number density causes total absorption.

The spectral intensity distribution of the white light source through the empty cell is first measured. After the intensity data is obtained, we place a sampled of Iodine in the cell. The power supply to the heater is turned on a left for around 10 minutes, which is when it reaches equilibrium. The temperature should never exceed the 30°C. Then me obtain the spectra for the Iodine and as extract an absorption graph.

5 Results and Discussion

5.1 Experiment 1

The first part of this section consisted of recording the different parameters and how these changed accordingly. These parameters are integration time, averaging, boxcar smoothing, and dark current correction.

Integration time refers to how long the detector monitors incoming photons. Using the automatic setting, the integration time was set to approximately 95,460 μs. Increasing the integration time beyond 100,000 μs led to saturation, where spectral peaks exceeded the detector's limits. Lowering the integration time below 10,000 μs resulted in poor signal intensity. The automatic setting can be seen in figure 4, saturation in 5, and poor signalling in 6.

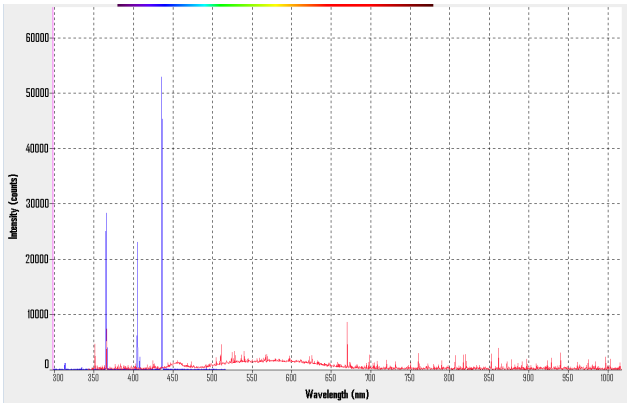

Figure 4: Spectrum of Mercury at 'automatic' integration time

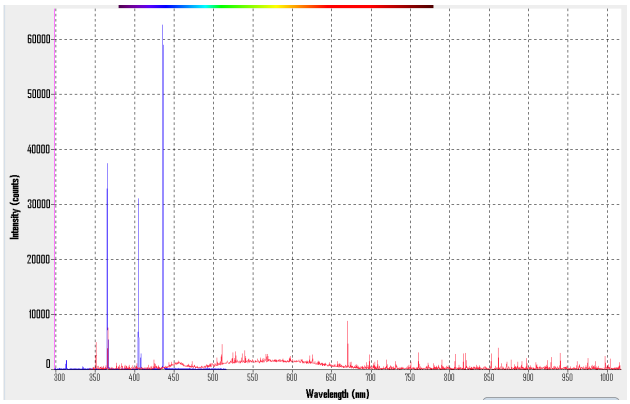

Figure 5: Mercury spectrum corresponding to 130,000 μs

Average refers to the number of scans produced in a single spectrum; it reduces the notice while increasing the acquisition time. When scan-to-average is set to 1, there is no averaging and data is returned as soon as it is available. This is instead set to 5 to balance both mentioned factors.

Boxcar smoothing is a technique that averages the spectral data. Initially setting it to 0 returns an observation of raw spectral data. A width of 5 was applied resulting in smoothing the spectral lines without losing

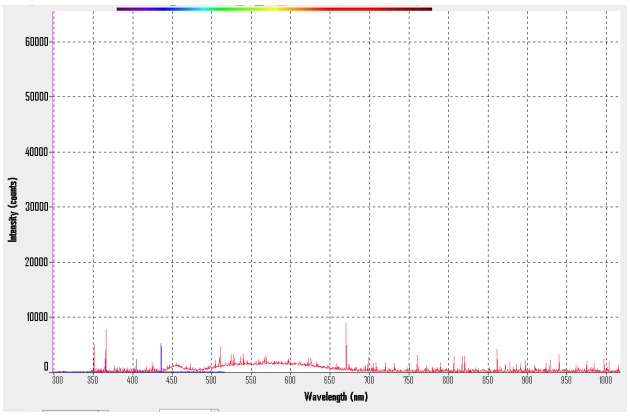

Figure 6: Mercury spectrum corresponding to 10,000 μs

resolution. Increasing the boxcar width beyond 8 caused excessive smoothing, distorting peak information. The loss of data resulting from the too-high values can be seen in Figure 7.

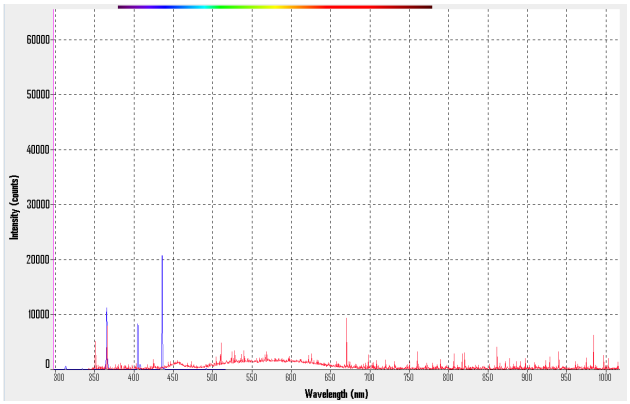

Figure 7: Mercury spectra for boxcar with width = 8

The final factor is the dark current correction, which enables or disables the correction of spectral data for electrical dark signal, which is essentially the noise caused by the detector and electronics. When disabled, the spectrum showed a baseline shift due to dark current noise (Figure 8). Otherwise, the noise was filtered, producing cleaner spectral data (Figure 9).

The alignment of the optical fiber relative to the mercury lamp was a significant factor when recording the spectra. When properly aligned, the spectra exhibited strong, well-defined peaks. Slight misalignment resulted in reduced peak intensity although the spectral features remained intact as seen in Figure 10. In contrast, extreme misalignment (Figure 11) resulted in immediate saturation, as excessive light entered the spectrometer which overwhelmed the detector. This highlights the importance of precise fiber positioning when performing spectroscopic measurements to ensure consistent and accurate spectral data.

The measured emission lines from the mercury discharge lamp were recorded and compared to reference values. The following peaks were identified using the Flame-T spectrometer:

The emission spectrum for the Flame-T spectrometer is seen in Figure 12.

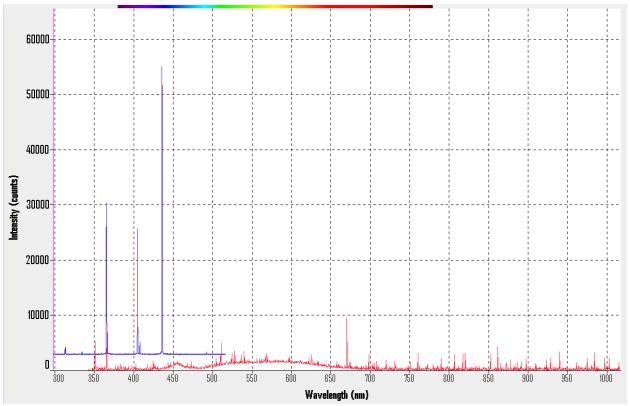

Figure 8: Mercury Spectra for 'electrical dark' disabled

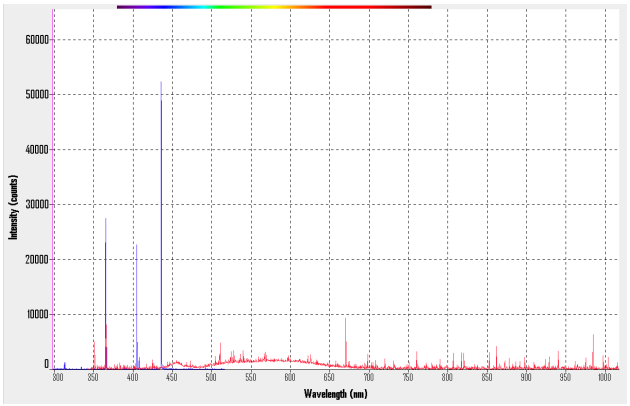

Figure 9: Mercury Spectra for 'electrical dark' enabled

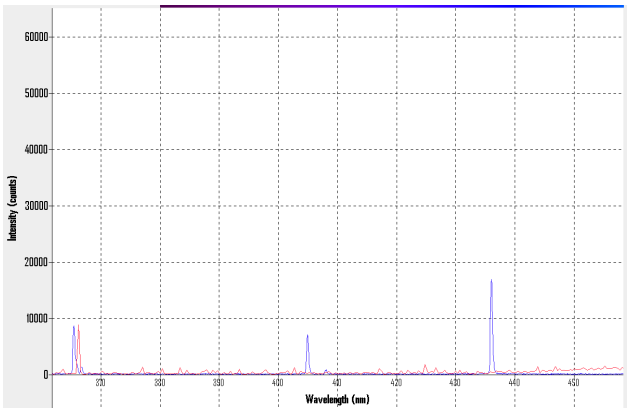

Figure 10: Mercury Spectra produced from slight misalignment

To find the resolving power, selected wavelengths and their corresponding FWHM values were used, which was found using the given software (Figure 13). The results are summarized in Table 3.

For the Flame-S spectrometer, additional longer-wavelength peaks were recorded, as seen in Figure 14. It

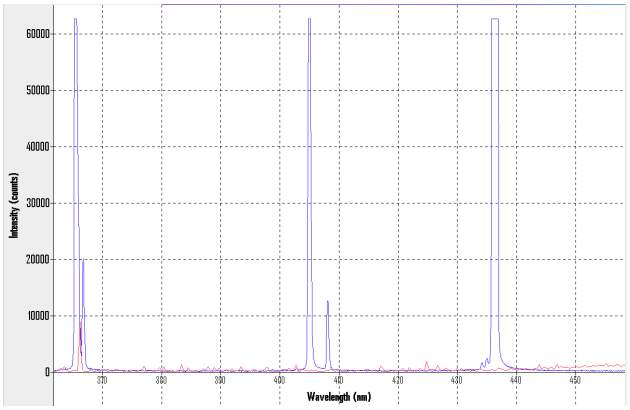

Figure 11: Mercury Spectra produced from extreme misalignment

Measured Wavelength (nm)	Reference Wavelength (nm)	Difference (nm)
365.457	365.48	-0.023
404.92	404.95	-0.03
436.23	436.27	-0.04

Table 2: Comparison of Measured and Reference Wavelengths for Flame-T

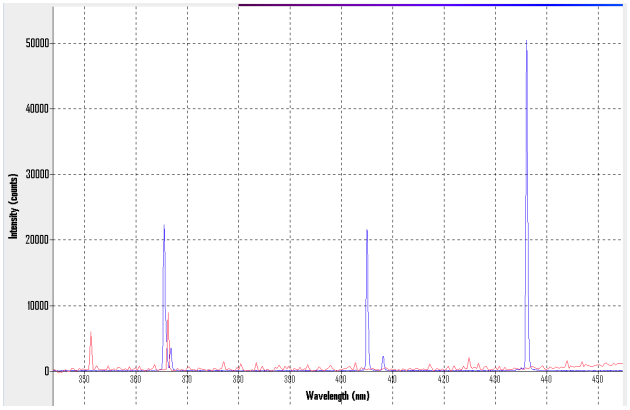

Figure 12: Emission spectrum for the Flame-T spectrometer

Wavelength (nm)	FWHM (nm)	R
313.61	1.03	304.47
321.08	0.49	655.27
365.47	0.57	641.17
404.93	0.52	778.71
436.07	0.49	889.93

Table 3: Sample data of wavelength, FWHM, and R.

can be observed again the close resemblance between the recorded values and the known reference wavelengths of mercury. The small differences are within the instrumental uncertainty, $+/-0.4$ nm.

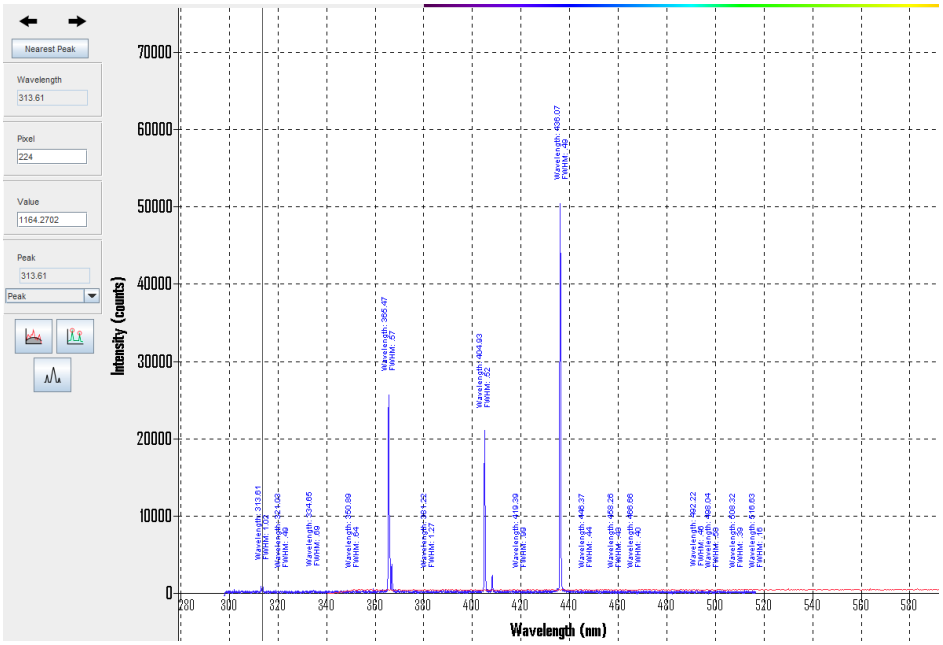

Figure 13: FWHM and peak values for Flame-T

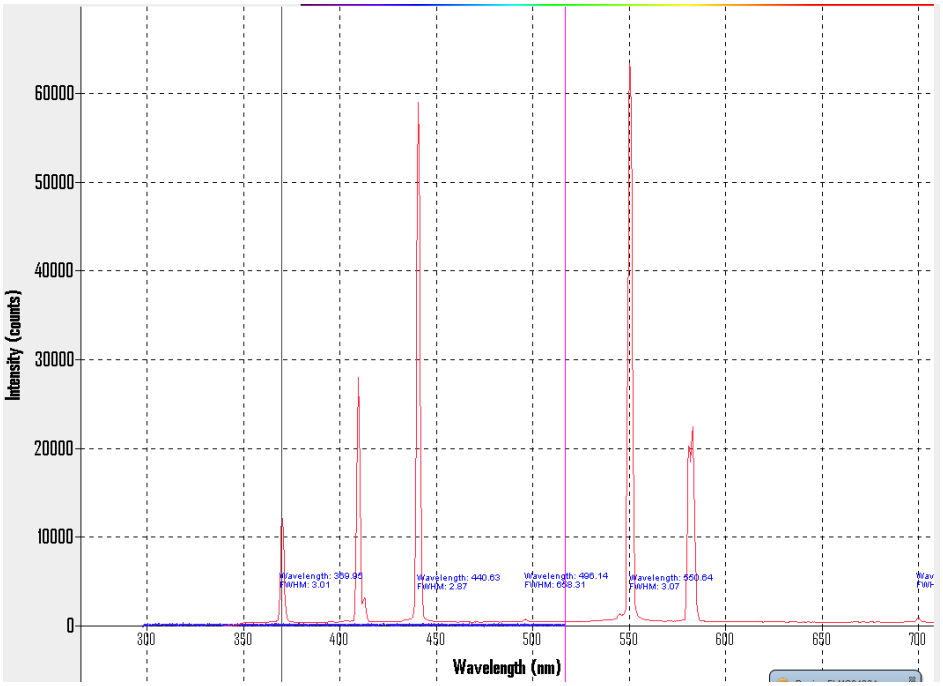

Figure 14: Emission spectrum for the Flame-S spectrometer with FWHM and peak values

From the gathered information, we can generate the resolving power table for the Flame-S spectrometer.

The Flame-T spectrometer, which operates in the 300–510 nm range, exhibited higher resolving power for shorter wavelengths. The recorded FWHM values were relatively low, leading to resolving power values in

Measured Wavelength (nm)	Reference Wavelength (nm)	Difference (nm)
546.08	546.07	+0.01
577.02	576.96	+0.06
579.07	579.07	0.00

Table 4: Comparison of Measured and Reference Wavelengths for Flame-S

Wavelength (nm)	FWHM (nm)	R
389.98	3.01	129.60
440.63	2.87	153.55
496.14	688.31	0.72
650.64	3.07	211.94

Table 5: Wavelength, FWHM, and Resolving Power Data for Flame-S

the range of 300–900, depending on the wavelength. For example, the doublet near 313 nm was successfully distinguished, confirming that the spectrometer can resolve closely spaced spectral lines in this region. The resolving power followed the expected trend, where resolution improves at longer wavelengths, although with diminishing returns.

The Flame-S spectrometer, covering a broader range of 350–850 nm, showed a more varied resolving power across different wavelengths. At shorter wavelengths (e.g., 389.98 nm, 440.63 nm), resolving power was within a reasonable range (approximately 130–210), indicating moderate resolution. However, at 496.14 nm, the FWHM was unexpectedly high (688.31 nm), resulting in an abnormally low resolving power (0.72). This suggests either instrumental broadening, saturation effects, or measurement errors at this wavelength. For longer wavelengths, such as 650.64 nm, the resolving power was relatively high ($\sim$212), confirming that the Flame-S spectrometer performs better in this region.

5.2 Experiment 2

The emission spectrum of Nitrogen was obtained using the Flame-T spectrometer in the 300–510 nm range. The data collection process followed the necessary optimization steps to ensure a clear and high-quality spectrum. The 0-0 vibrational transition was expected to be the most intense peak, reaching approximately 50,000 counts, as indicated in the lab manual. Initial spectra showed lower-than-expected peak intensities, which were later corrected by increasing the integration time to capture more photons. The corresponding spectra of Nitrogen is displayed in Figure 15.

Figure 16 resulted in the increase of integration time to increase the resolution for the lower peak values for observational purposes.

Once the spectrum with the optimized settings was obtained, distinct peaks corresponding to vibronic transitions were identified. We can analyze these peaks and assign them their corresponding vibrational levels by referencing the Franck-Condon factors table (Table 1) and keeping in mind Figure 2, which explains the relative intensity of transitions based on vibrational wavefunction overlap. The most prominent peak is the one that corresponds to the 0 - 0 transition, observed at 336.89 nm. Taking into account the fact of vibrational progression and that transitions with lower Franck-Condon factors have lower intensities, we can assign the mentioned transitions to the distinctive peaks seen in the spectra. Table 6 is an assertion of these

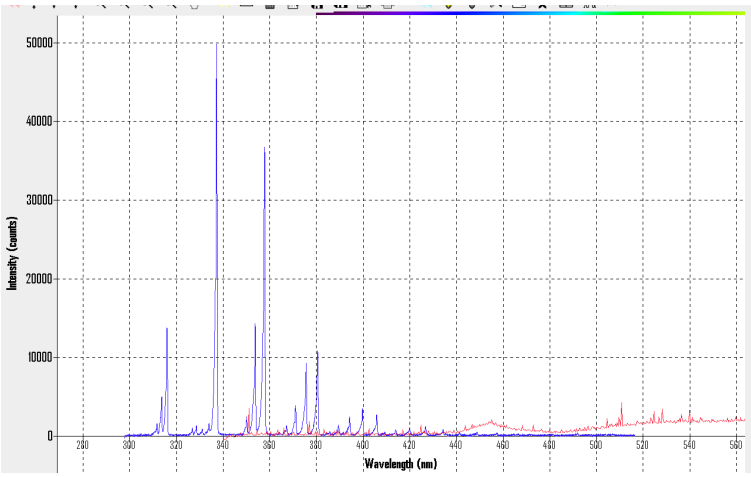

Figure 15: Emission spectra with 'automated' integration time

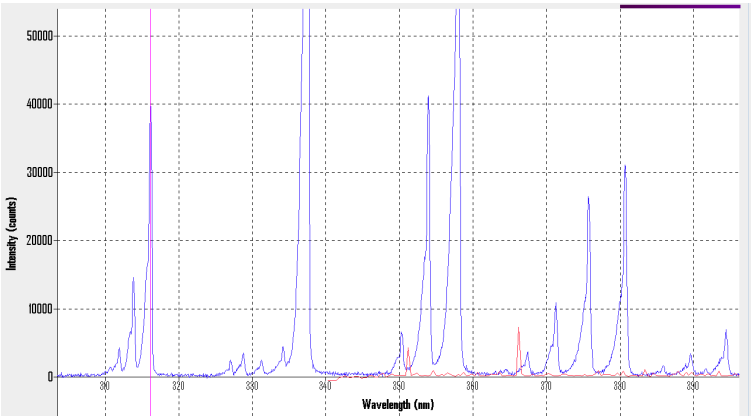

Figure 16: Long-exposure spectrum to view low-intensity features

values and the following Nitrogen spectra in Figure 17 has the labelled peaks.

Wavelength (nm)	**Vibrational Transition** ($\nu' \to \nu''$)	ν' (cm^{-1})
336.89	$0 \to 0$	29761.9
358.08	$0 \to 1$	27926.17
380.71	$0 \to 2$	26266.436
394.43	$0 \to 3$	25352.85
316.12	$1 \to 0$	31634.06
353.67	$1 \to 1$	28274.87
375.67	$1 \to 2$	26618.97

Table 6: Wavelengths and Corresponding Vibrational Transitions

Based on these approximations we can build the corresponding Deslandres Table, as seen in Table 7. A sample calculation of the obtained table goes as follows.

$$\Delta\tilde{\nu}(v' - v'') = \tilde{\nu}(v', v'') - \tilde{\nu}(v', v'' + 1) \tag{21}$$

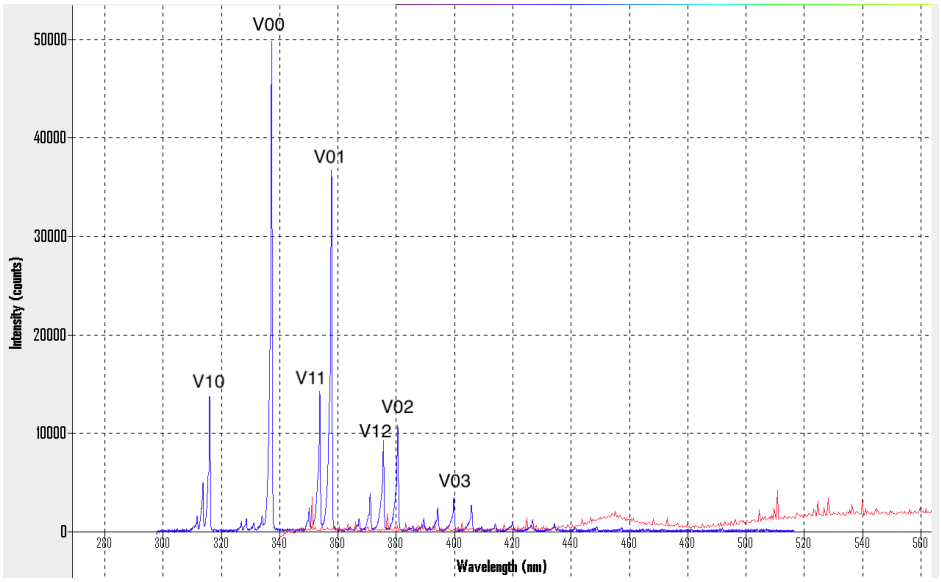

Figure 17: Emission spectra with labelled vibrational transitions

ν'/ν''	0	$\Delta\tilde{\nu}(0-1)$	1	$\Delta\tilde{\nu}(1-2)$	2	$\Delta\tilde{\nu}(2-3)$	3
0	29761.9	1835.73	27926.17	1659.73	26266.44	913.59	25352.85
1	31634.06	3359.19	28274.87	1655.90	26618.97	-	-

Table 7: Deslandres Table

For $v' = 0$:

$$\begin{aligned}\Delta\tilde{\nu}(0-1) &= \tilde{\nu}(0,0) - \tilde{\nu}(0,1) \\ &= 29761.9 - 27926.17 = 1835.73(cm^{-1})\end{aligned}$$

One of the remarks we can give is the decrease of the energy spacings. The $\Delta\tilde{v}$ value decreases as the vibrational quantum number increases, which confirms the anharmonicity in the nitrogen molecule. This is because as the mentioned values decreases along with higher vibrational states, the energy differences between successive levels shrink which is a clear sign of anharmonicity. This can be more physically understood by looking at Figure 2, which shows the decreasing distance between the energy levels as the quantum number increases. Anharmonicity happens due to the fact that real molecules do not behave like ideal springs. As vibration increases, the bond stretches further than it compresses, leading to a decrease in restoring force. If nitrogen behaved as a perfect harmonic oscillator, then the differences $\Delta\tilde{v}$ would be constant.

Additionally, the smooth numerical decrease confirms that the labeled transitions are correct as if a peak had been misidentified, the energy gaps would be inconsistent. It also shows consistency with the molecular vibration theory, as higher vibrational transitions experience reduced spacing.

5.3 Experiment 3

The first parameter we adjusted was the integration time. As previously done, we find that increasing it too much causes saturation (3000 microseconds), while an excessively low value (1000 microseconds) does not yield enough information. The automated number is set to 2060 microseconds. Saturation occurred at around 2740 microseconds. The scans-to-average is increased to 32, which provides notoriously smoother data. This continuity is enhanced by setting the boxcar width to 5. Finally, the electrical dark option is enabled to get rid of the possible excess noise.

The position of the lamp is adjusted to increase the number of photons detected by the spectrometer, the same as in the mercury lamp. The resulting spectrum is displayed in Figure 18. The recorded emission spectrum of the tungsten-halogen lamp exhibits a characteristic broadband distribution, with intensity peaking around the 600–700 nm range before gradually decreasing toward both lower (blue) and higher (infrared) wavelengths. This distribution aligns well with the expected behavior of a blackbody radiator, where the intensity follows Planck's radiation law. Fluctuations can be attributed to the fact that the sensitivity of the spectrometer varies with wavelength, so it is not perfect.

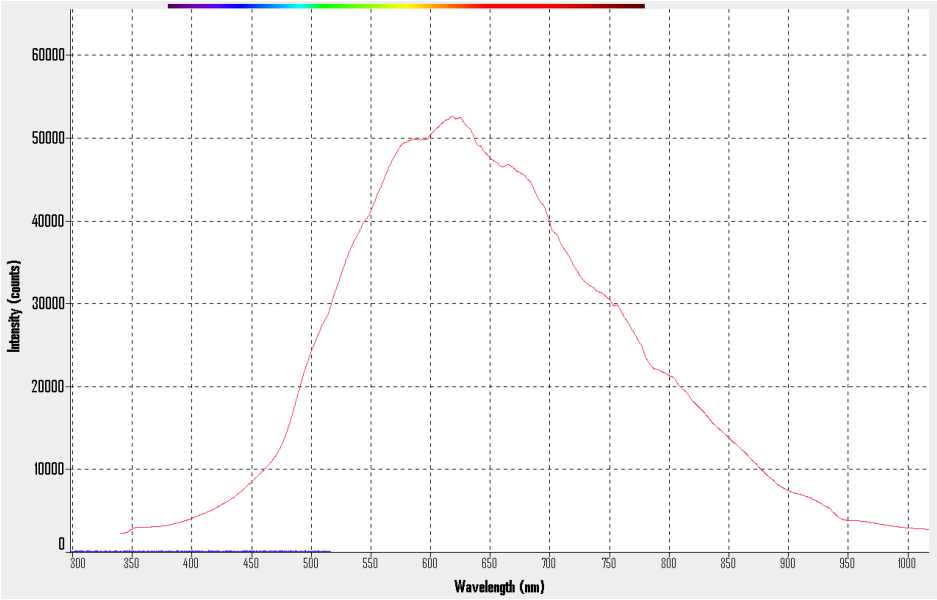

Figure 18: Emission spectrum of a continuum white light source

The intensity and wavelength data are drawn from this to find the blackbody intensity spectrum (Figure 19) and sensitivity plot (Figure 20). The blackbody radiation curve shown in the third plot provides a theoretical reference for how the tungsten filament should behave, with the expected increase in intensity as wavelength increases. The final plot of sensitivity vs. wavelength for the spectrometer provides important insights into potential distortions in the recorded emission spectrum. The response is not uniform across all wavelengths, as we can observe it exhibits higher sensitivity in the mid-visible range (around 550–750 nm) and lower sensitivity at shorter and longer wavelengths. Mid-visible wavelengths may be more emphasized due to the higher spectrometer efficiency in that range. Near-infrared and UV regions might be underrepresented due to lower detector sensitivity. Finally, the observed decrease in the blue region (around 400 nm) may

reflect the actual lamp spectrum while also being influenced by the instrument's reduced detection efficiency at shorter wavelengths.

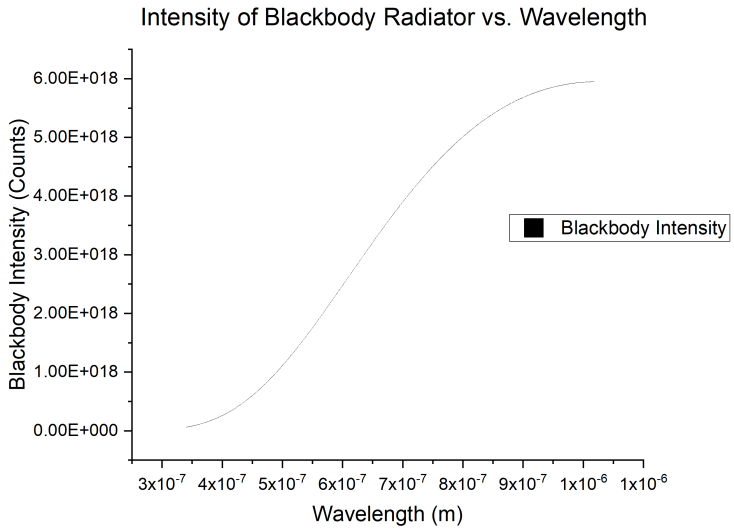

Figure 19: Intensity as a function of wavelength (Planck's formula)

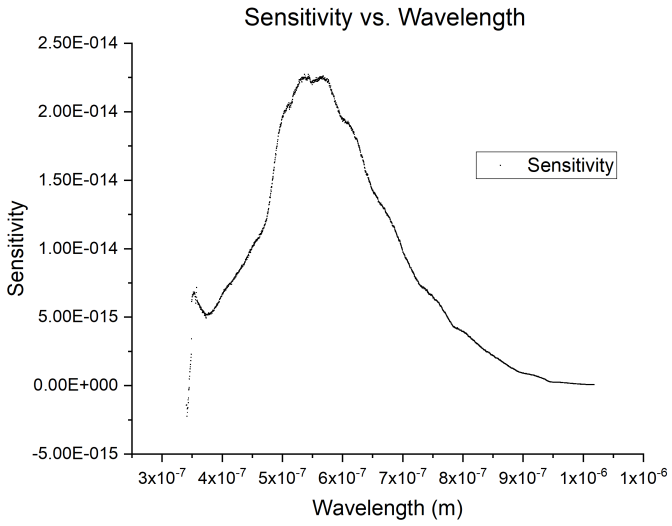

Figure 20: Sensitivity vs. Wavelenght

5.4 Experiment 4

The experiment aimed to record and analyze the absorption spectrum of iodine by measuring the transmitted intensity against the reference intensity. The results obtained, however, exhibited irregularities, which are likely attributed to incomplete heating and external interferences that affected the measurement conditions.

The recorded intensity spectra, both with and without the iodine cell, show clear intensity fluctuations across different wavelengths. However, when analyzing the absorbance spectrum, the expected well-defined vibrational bands were not distinctly observed. Instead, the absorption features appeared weaker than anticipated, with a noticeable deviation from the reference spectra of iodine at elevated temperatures.

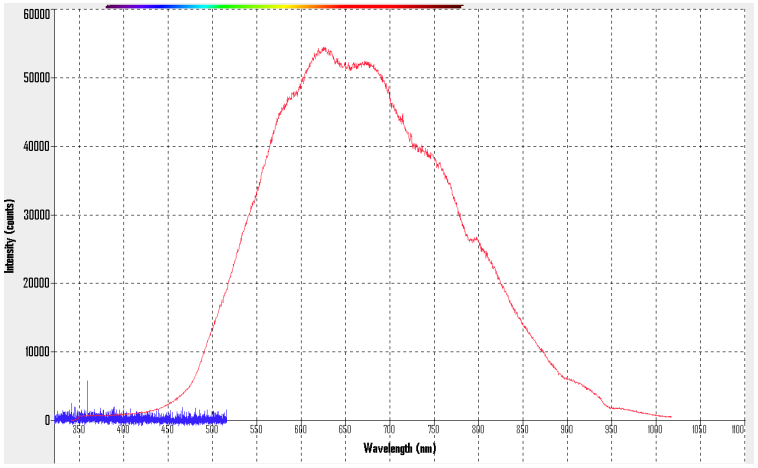

Figure 21: Intensity Spectra of Empty Iodine Cell

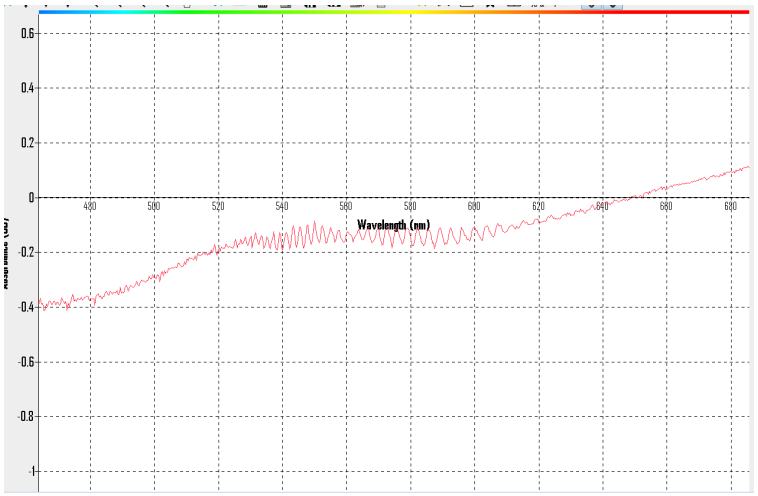

Figure 22: Spectra of Heated Iodine Cell

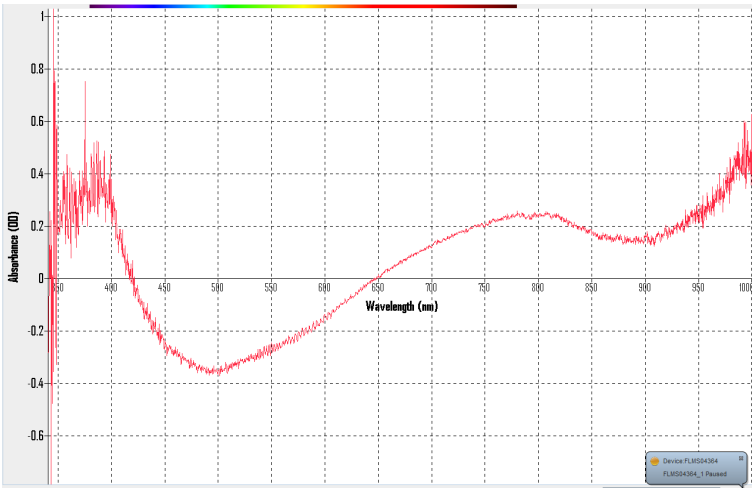

Figure 23: Zoomed out Spectra of Heated Iodine Cell

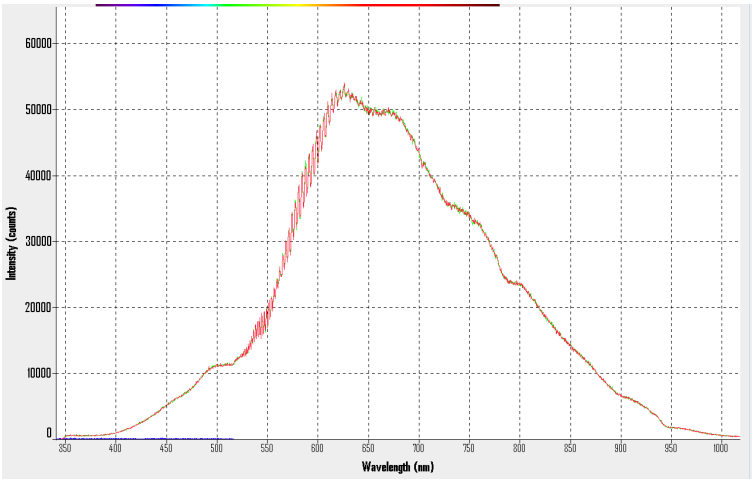

Figure 24: Intensity of Heated Iodine Cell

Figures 22 and 23 are the absorption spectra of the heated iodine. In comparison, the graph in Figure 25 shows a typical iodine absorption spectrum after proper heating, exhibiting well-defined vibrational progression due to transitions between the ground electronic state and an excited electronic state. The experimental spectra recorded in the lab do not fully resemble this expected result, which suggests that the iodine vapor might not have reached an optimal temperature for full vaporization. This incompleteness would result in a lower population of iodine molecules in the absorbing state, reducing the clarity of observed vibrational bands.

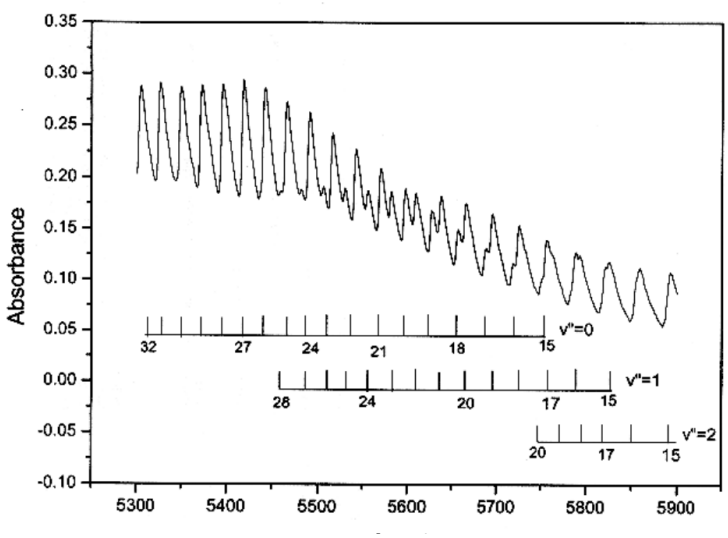

Figure 25: Reference of Absorption Spectrum of I_2. Numbered scales represent vibrational level assignments. (Trinity College Dublin, 2023).

Limitations during this section of the laboratory, including the lack of time to repeat the initial absorption spectra and fix the flawed obtained heated iodine spectrum, prevented the further investigation of the iodine absorption spectrum and its comparison between the intensity before heating the iodine cell. When heating the iodine cell we encountered the unusual pace of increasing temperature, which exceeded the allowed value of 30°C. Inconsistencies in this process and lack of clarity for obtaining the data prove to be a limit on the analysis required.

6 Conclusion

This experiment analyzed the emission spectrum of nitrogen and the absorption spectrum of iodine, providing insights into molecular transitions. The nitrogen spectrum confirmed vibrational energy spacing reduction, consistent with anharmonicity, while intensity variations aligned with Franck-Condon factors. The iodine absorption spectrum, though affected by heating inconsistencies, still highlighted electronic excitation transitions.

Additionally, the continuum emission spectrum of a tungsten-halogen lamp was recorded and compared to blackbody radiation, revealing instrumental response variations. The findings reinforce the importance of the presence of vibrational transitions in molecular behavior and highlight the need for precise experimental conditions to improve spectral resolution.

7 References

Atkins, P. W., & Friedman, R. S. (2005). Quantum mechanics (5th ed.). Retrieved 03/02/2025. Stanford University. https://web.stanford. edu/ oas/SI/QM/Atkins05.pdf.

Bersohn, R., & Berne, B. J. (2003). Chemical Physics. Retrieved 03/02/2025. Elsevier EBooks, 739–749. https://doi.org/10.1016/b0-12-227410-5/00099-5.

Herzberg, G. (1950). Molecular Spectra and Molecular Structure: I. Spectra of Diatomic Molecules. Retrieved 03/02/2025. National Research Council of Canada. Van Nostrand Reinhold Inc.

JPierce. (2017, March 19). What is a Czerny-Turner Configuration? - StellarNet, Inc. Retrieved 05/02/2025. StellarNet, Inc. - StellarNet, Inc. website: https://www.stellarnet.us/what-is-a-czerny-turner-configuration/

Trinity College Dublin (2023). Retrieved 03/02/2025. Junior Sophister Laboratory: Molecular Spectroscopy.